The role of tungsten chemical state and boron on ammonia formation using N_2-H_2 radiofrequency discharges

R Antunes[1], L Marot[1], C Romero-Muñiz[2,3], R Steiner[1], E Meyer[1]

[1] Department of Physics, University of Basel, Klingelbergstrasse 82, CH-4056 Basel, Switzerland

[2] Department of Physical, Chemical and Natural Systems, Universidad Pablo de Olavide, Ctra. Utrera km. 1, E-41013, Seville, Spain

[3] Departamento de Física Aplicada I, Universidad de Sevilla, E-41012, Seville, Spain

E-mail: `rodrigo.antunes@unibas.ch`

Abstract. This work aims at investigating the role of tungsten and boron surfaces on ammonia production with N_2-H_2 radiofrequency plasmas at 3 Pa. The experiments combine the analysis of the reaction products and surface chemical environment using mass spectrometry and X-Ray Photoelectron Spectroscopy. We show that NH_3 is formed upon discharges of N_2 or H_2 after having exposed a tungsten (W) foil to H_2 or N_2, respectively. A higher amount of ammonia is formed for the N_2-then-H_2 case, which we explain by the larger number of Eley-Rideal reaction channels for the formation of NH_x(s) and the lower surface diffusion barrier for adsorbed hydrogen, calculated using the Density Functional Theory (DFT). As a result, H(s) combines with N(s) or NH_x(s) through Langmuir-Hinshelwood at a faster rate than N(s) combines with another N(s). The amount of NH_3 formed with N_2-H_2 discharges after conditioning the tungsten foil with H_2, N_2 or O_2 was also investigated. We observed that this pre-conditioning plays no major role on the amount of NH_3 detected with the Residual Gas Analyser, albeit a small decrease was observed after H_2 contamination. With DFT, the adsorption energies of H on WO_3 and W are found to be similar, while the adsorption of N on WO_3 is significantly weaker. The similar NH_3 concentrations obtained with a clean and oxidized tungsten surface thus suggest that the adsorption of N does not limit the formation rate of ammonia. The production of NH_3 on boron was evaluated as well. The boron surface reduced the amount of detected ammonia almost by half. On the one side, a significant amount of H_2 was removed from the surface during Ar cleaning, which suggests a strong retention of hydrogen. On the other side, the XPS data reveals that nitrogen forms strong bonds with boron and impurities on the surface, regardless on whether hydrogen is previously present on the surface or in the plasma volume. The presence of hydrogen in the plasma volume, simultaneously with nitrogen or after nitrogen exposure, is nevertheless necessary for the formation of NH and NH_2. No NH_3(s) was however detected with XPS. The increased retention of both hydrogen and nitrogen on the surface may thus hinder the formation of NH_3.

Keywords: ammonia, radiofrequency plasmas, tungsten, boron

1. Introduction

The divertor is a major component of the ITER fusion reactor as it is designed to cope with large heat and particle fluxes [1]. During ITER operation, stationary power fluxes on the tungsten (W) divertor are expected to reach $10\,\mathrm{MW\,m^{-2}}$. To ensure that this limit is not exceeded, impurities will be injected to radiatively spread the plasma heat over a larger area [2]. Argon (Ar), neon (Ne) and nitrogen (N_2) are currently envisaged to be used as seeding species to fulfill this task. The latter appears to be the most suitable species due to its radiative properties, and previous experiments with the full-tungsten ASDEX Upgrade (AUG) tokamak have demonstrated a higher energy confinement when N_2 was added to a deuterium discharge [3]. However, the use of nitrogen may negatively impact the fuel cycle and management of a fusion reactor. On the one side, the formation of tungsten nitride layers has been observed to enhance the retention of deuterium [4]. On the other side, the dissociation into atomic N in a hydrogen-isotope plasma will lead to the formation of ammonia isotopologues NQ_3, where Q = H, D, T (protium, deuterium, tritium). Such observations in the fusion community were first reported after seeded and subsequential non-seeded discharges in AUG [5]. The formation of ammonia was also observed during JET ITER-like wall discharges, whereby the issue of catalysed production of ammonia due to the presence of metallic plasma facing components was raised [6, 7]. Since ammonia is a polar molecular, it will unavoidably stick onto ITER walls, which will be made of beryllium (first wall), tungsten (divertor) and stainless steel (pumping ducts of the vacuum vessel) [8]. Consequently, the formation of large quantities of tritiated NQ_3 will impact ITER operation and maintenance since the in-vessel tritium inventory must not exceed 1 kg at all times [9]. Moreover, the presence of ammonia in the exhaust stream impacts the design of the ITER Tokamak Exhaust Processing (TEP) system, which will be responsible to detriate the incoming gas mixtures [10, 11]. Therefore, it is of paramount importance to understand the underlying mechanisms of ammonia formation and identify strategies to efficiently destroy it.

The formation of NH_3 in the presence of N_2-H_2 plasmas has received increasing attention within the low-temperature plasmas community. Several research groups reported the production of ammonia with different types of discharges, including dielectric barrier discharge (DBD), glow discharge (GD) and radiofrequency (RF) [12–14]. The wide range of catalytic performances obtained with various materials highlight the importance of surface reactions [15, 16]. Several simulation studies have underscored the importance of the so-called Eley-Rideal (E-R) and Langmuir-Hinshelwood (L-H) reaction mechanisms between N and H to form NH(s), a key precursor of NH_3 [15, 17–20]. Iwamoto et al. showed that in atmospheric plasmas the formation rate of NH_3 is lower for surfaces onto which N is more strongly bound. In contrast, Shah et al. proposed three competing rate-limiting steps in low-pressure plasmas: surface recombination of H into H_2, H diffusion into the bulk and N-H formation on the surface. A recent work, combining experiments with *ab initio* molecular

dynamics, showed that the mechanisms for NH_3 formation at low pressures depend on the N adsorption energy [21]. Having a lower adsorption energy, N hardly adsorbs on copper (Cu) and the formation of NH_3 is a result of N bombardment onto a copper H-terminated surface. In contrast, for platinum (Pt), with a high N adsorption energy, Yamijala et al. showed that the saturation of the surface with NH groups is necessary to allow NH_3 formation. Despite the different mechanistic processes, the formation of NH_3 was found to be not significantly different for both metals.

The catalytic performances of tungsten have been studied using different experimental facilities. Using GD plasmas, de Castro et al. reported an increase of the ammonia yield with both the increase of N_2 in the plasma and the temperature of the tungsten wall [22]. This study also discusses the formation of tungsten nitrides with W:N ratios larger than 1:1 and 2:1, corroborating the results obtained by L. Laguardia et al. who observed the formation of W_xN_y layers with D_2-N_2 RF discharges using GyM [23]. de Castro et al. also reported the positive impact of adding He into the plasmas as well as the increase of the residence time of N_2 on the NH_3 yields [24, 25]. Instead, L. Laguardia et al. reported the reduction of ND_3 formation in N_2-D_2 plasmas in the presence of helium and argon [26], whereas Ben Yaala et al. observed opposing tendencies [27]: while the increase of He led to a net reduction of detected NH_3, Ar contributed to a slight increase of ammonia, possibly due to the impact of Ar^+ ions on the plasma chemistry and properties (namely the increase in the density of dissociated N atoms and electron density). Moreover, the amount of NH_3 adsorbed on the tungsten surface was found to decrease with both He and Ar. Recent works from our group showed that the NH_3 formation rate is highest in the presence of an equimolar mixture of N_2-H_2 at a few Pa and 120 W [28,29]. Furthermore, the NH_3 production was observed to increase by a factor of 2 from 30 to 120 W, whereas the increase in pressure beyond 3 Pa had a detrimental effect due to a decrease in the electron temperature.

In this study, we aim at evaluating the catalytic performances of tungsten and boron when subject to various fusion-relevant plasmas. To gain better insights into our main results, in the first part of this work we combine Ar^+ bombardament with Thermal Desorption Spectroscopy (TDS) to evaluate the species adsorbed on the reactor/tungsten walls and those diffused into the W bulk after contamination with a Residual Gas Analyser (RGA). In the second part, the data obtained with the RGA and X-Ray Photoelectron Spectroscopy (XPS) are combined to study the reaction products and the surface chemical environment of tungsten and boron surfaces exposed to N_2, H_2 or N_2-H_2 plasmas. Furthermore, H_2, N_2 and O_2 plasmas are used to saturate the tungsten surface prior to N_2-H_2 discharges. The catalytic behavior of tungsten oxide is of interest for the fusion community, since the combination of oxygen and high temperatures or coolant loss (steam ingress) events may lead to the oxidation of the W divertor [30, 31]. The experiments with boron aim at reproducing the so-called boronization, whereby the tokamak is coated with B to reduce the amount of plasma impurities, namely C or O [3].

2. Experimental setup and procedure

The ammonia production experiments were carried out with a surfatron plasma source connected to the gas supply side of a 1400 mm-long pyrex cylindrical tube (inner diameter: 31 mm). The exhaust side was attached to a high-vacuum chamber, inside which an RGA was installed. A 0.05 mm-thick tungsten foil (99.7 wt% purity, Plansee SE), with a surface area of 500 cm^2 (whereas the glass chamber has total of 1700 cm^2) and roughness R_a of 80 nm, was placed inside the pyrex tube, in the same region where an oven (Nabertherm GmbH) was also employed. The plasma discharges were produced with a 13.56 MHz RF generator in combination with a matching box (Hüttinger GmbH and Co KG, PFM 1500A). All gases used in the experiments (H_2, N_2, O_2, Ar) were of high purity (99.9999%). A more detailed description of the setup, referred to as "ammonia chamber", is provided in [29].

Two main experimental procedures were followed in this work. The first concerned analysing the species being desorbed from the reactor walls (tungsten + pyrex) after exposing them to plasmas of single gases (H_2, N_2, O_2) or mixtures (N_2-H_2). This analysis combined Ar^+ sputtering (referred to as Ar cleaning) with TDS. The Ar^+ ions were generated at 0.6 Pa and with an RF power of 120 W, corresponding to an ion energy of $\approx$ 20 eV, given by the difference between the plasma and floating potentials measured by a Langmuir probe. Ar cleaning is a typical procedure carried out after exposing the chamber to air (e.g., insertion of a new sample), ensuring a low amount of impurities on the reactor and tungsten walls. TDS was carried out from room temperature (RT) up to 673 K at a rate of 4 K min^{-1}, whereby the highest temperature was limited by the working temperature of pyrex. In the second set of experiments, we studied the formation of ammonia after conditioning the reactor walls with H_2, N_2 or O_2 plasmas at 3 Pa, using the RF power and temperatures displayed in table 1. The production of NH_3 was investigated with H_2, N_2 or 50-50 mol% N_2-H_2 plasmas generated with an RF power of 120 W at 3 Pa and RT. The formation of NH_3 was also studied on a boron surface, after coating ex-situ a tungsten foil with a

NH_3 formation plasmas	**H_2 contamin. plasma**	**N_2 contamin. plasma**	**O_2 contamin. plasma**	**B coating**
N_2 alone	60 W, RT			
H_2 alone		60 W, RT 300 W, 673 K		
N_2-H_2	60 W, RT	300 W, 673 K	300 W, 673 K	Magnetron sputtering

Table 1: Parameters used for the contamination of the reactor walls with H_2, N_2 and O_2 plasmas. All plasmas were generated at 3 Pa. The contamination plasmas were run for 2 hours. The NH_3 formation plasmas were ignited at RT and with 120 W of RF power.

several nm-thick boron layer by means of magnetron sputtering [32]. In-situ and ex-situ XPS studies were carried out as well to support the main observations presented and discussed in this work. The procedure used to prepare the samples as well as relevant data are given in the Supporting Information (SI). It is worth to point out that transferring the plasma-exposed sample to the XPS chamber, without ever breaking the vacuum, takes approximately 30 min, and only the species adsorbed on the surface are measured. In the ammonia chamber, Ar cleaning and TDS were systematically used to analyse the species desorbed from the surface and the bulk. They are meant to provide qualitative information only and they are not used to accurately estimate the inventory of the tungsten and boron foils.

3. Analysis of the species desorbed from the reactor walls

The species desorbed during Ar cleaning and TDS were evaluated by following the RGA signals of the relevant species. All the peaks of interest concern the m/z values of H, H_2, N, N_2 and their combinations in the form of NH_x, as summarized in Table 2. With our RGA, however, we cannot resolve $m/z = 1$ that would correspond to atomic H. H_2O and CO, and CO_2 in a lesser degree, were also observed to be removed from the walls after subjecting them to O_2 plasmas. Throughout the entire experimental campaign, no volatile species were detected after plasma exposure, which means that the species formed in the discharges were either adsorbed on the surface of the pyrex + tungsten (detected during Ar cleaning) or diffused into the W bulk (detected during TDS).

3.1. H_2-N_2 plasmas

Figure 1 presents two plots obtained after a typical experiment carried out with an equimolar plasma of N_2-H_2 at 3 Pa and 120 W of RF power. These results were obtained with Ar cleaning (left) followed by TDS (right). During Ar cleaning the main species

m/z	**Species**
2	H_2
14	N
15	NH
16	NH_2, O
17	NH_3, HO
18	NH_4^+, H_2O
28	N_2, CO
32	O_2
40	Ar
44	CO_2

Table 2: Relevant m/z ratios and species detected by the RGA.

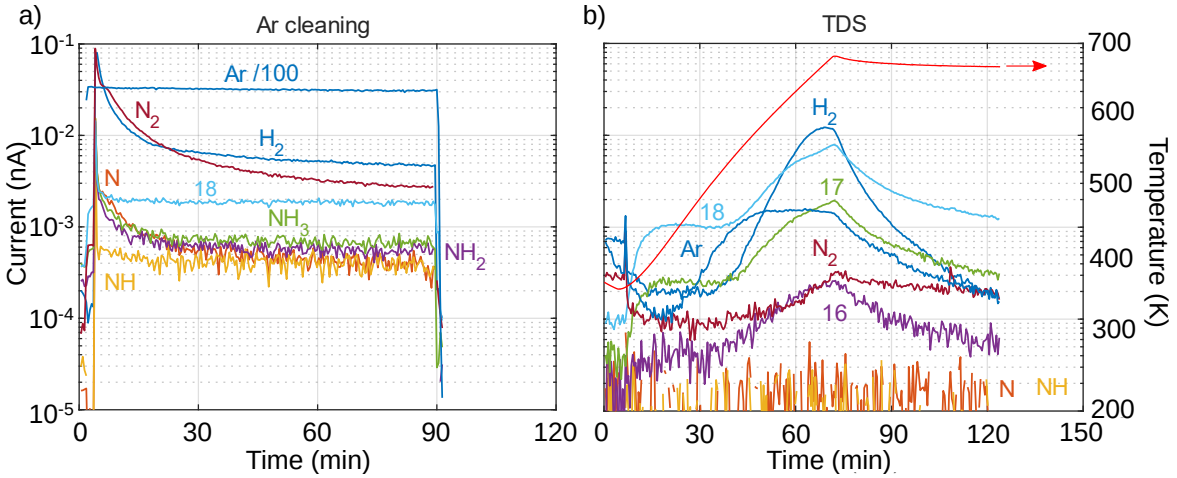

Figure 1: RGA signals for the relevant species obtained during Ar cleaning (left) followed by TDS (right). These plots were obtained after a 50-50 mol% N_2-H_2 plasma at 3 Pa and 120 W of RF power. The Ar^+ signal on the left plot was divided by 100 for better visualization.

removed are H_2 and N_2. We also observe that N, NH_3 and NH_2 are sputtered away during the process (although a significant contribution for N and NH_2 come from the cracking of N_2 and NH_3 at the RGA), whereas NH remains rather constant at background levels (refer to section S1 in SI). The presence of NH_x compounds on a pristine W surface after exposing it to 50-50 mol% N_2-H_2 with an RF power of 120 W and 3 Pa is confirmed with XPS (Figure S9 and S10), corroborating previous results from our group [28] obtained at 1.2 Pa and 10 mol% N_2. The peak 18 (NH_4^+, H_2O) remains unaltered at its typical background value (less than 1%). The TDS that followed shows H_2 increasing considerably beyond 500 K, while N_2 remains about 1 order of magnitude below. In contrast, the peaks 16, 17 and 18 are observed to increase in a similar fashion, suggesting the breaking of H_2O (into HO and O) at the spectrometer. The occurrence of H_2O may be due to the presence of H (from the N_2-H_2 plasma) and residual O in the bulk of the tungsten foil (below 0.01 wt%, according to the manufacturer).

The species adsorbed on the reactor's surface and diffused into the bulk of the tungsten foil were compared after N_2-H_2 plasmas generated with 60, 120 and 300 W. The following two procedures were carried out: N_2-H_2 plasma → Ar cleaning → TDS and N_2-H_2 plasma → TDS → Ar cleaning. The background discounted RGA signals were integrated over the time of the process for an evaluation of the main species removed. The results are presented in Figure 2. During Ar cleaning, H_2 and N_2 are the most important species to be sputtered away, whereas H_2 and H_2O are the dominant species desorbed during TDS. Generally speaking, the amount removed from the walls increases with the RF power used during an N_2-H_2 discharge due to the higher concentration of atomic species generated in the plasma volume. Furthermore, the comparatively large values obtained for H_2 and H_2O detected after the 300 W plasma suggest that a larger

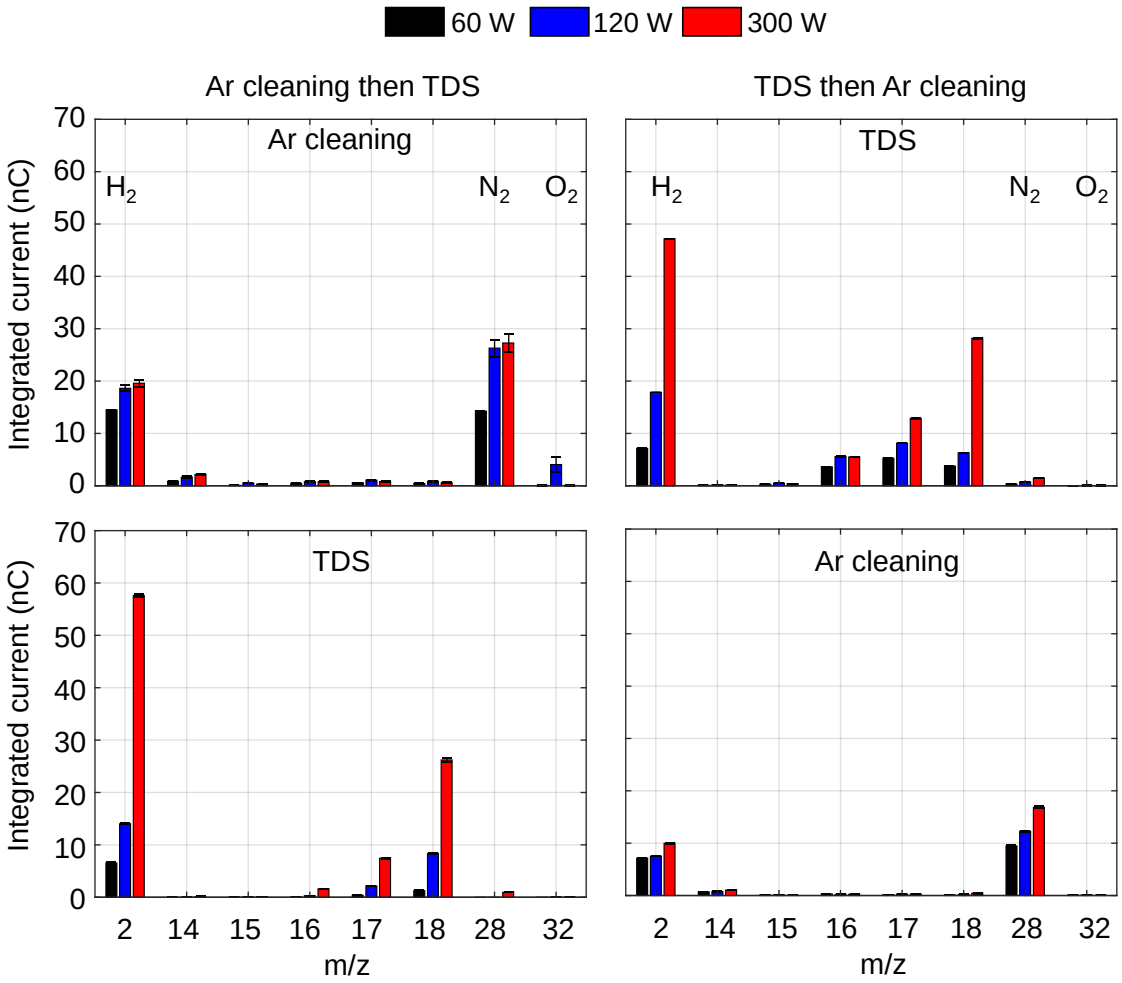

Figure 2: Integrated current obtained after N_2-H_2 plasmas generated with 60 W (black), 120 W (blue) and 300 W (red) at 3 Pa. The left-hand side plots were obtained with Ar cleaning followed by TDS, whereas the plots on the right were obtained with TDS followed by Ar cleaning.

amount of atomic H has diffused into the W bulk. The removal of N and N_2 takes place mostly during Ar cleaning, which is explained by two factors: (1) the negligible diffusivity of N below 600 K [33, 34], which implies that these species are implanted on the tungsten surface, and (2) the stability of nitride phases (e.g., W_2N) up to 600 K, and thus only a small increase of the N_2 signal is expected along our TDS procedure, as displayed in Figure 1b) [34–36]. The steady-state ammonia generated with 60 W, 120 W and 300 W N_2-H_2 plasmas was not affected by the order of the Ar cleaning and TDS procedures.

3.2. H_2, N_2 and O_2 plasmas

The saturation of the reactor walls with H_2, N_2 and O_2 plasmas was done at various conditions of temperature, exposure time and plasma power. Subsequently, Ar^+

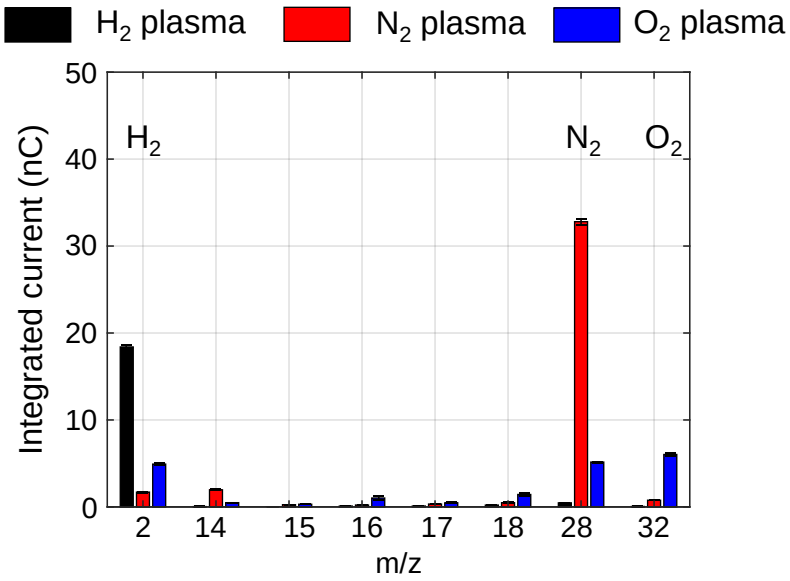

Figure 3: Integrated current obtained during Ar cleaning after subjecting the reactor walls to H_2, N_2 and O_2 plasmas. Contamination carried out with H_2 (RT, 60 W, black), N_2 (673 K, 300 W, red) and O_2 (673 K, 300 W, blue) plasmas at 3 Pa.

bombardment followed by TDS were done to evaluate the removed species. Figure 3 displays the results obtained during Ar^+ exposure. As expected, the species removed from the tungsten surface correspond to those present in the plasmas, with a clear predominance of the molecular form.

After exposing the reactor to various N_2 plasmas, the amount of species desorbed during Ar cleaning and TDS was rather similar, regardless of the exposure time, temperature and RF power (Figure S3). In contrast, the sputtering of hydrogen from the reactor walls after H_2 plasmas was found to be highly dependent on the temperature at which the contamination took place: the amount removed during Ar cleaning was higher for a plasma at RT and 60 W than at 673 K and 300 W, despite the higher concentration of H atomic in the plasma volume at larger powers. The same trend was observed during TDS, i.e. the amount of desorbed H was significantly lower with the latter conditions (Figure S4). During TDS, the increase in the $m/z = 2$ signal shifted from $\approx$ 500 K, for the H_2 plasma at RT, to $\approx$ 600 K, for the plasma at 673 K (Figure S5). These observations are consistent to those recently reported with deuterium plasmas, whereby the D inventory in W was found to be quite stable with plasma exposure up to 500 K [37]. At higher temperatures, the D retention decreases significantly, accompanied by a shift in the desorption peak towards higher temperatures. Similarly, Alimov et al. reported that the highest retention of D in tungsten is achieved at $480 - 530$ K [38].

Comparatively larger amounts of H_2O (peak 18), CO (peak 28) and O_2 (peak 32) were detected along Ar^+ bombardment after exposing the reactor walls to a 2 h-long O_2 plasma at 673 K and 300 W. The formation of these species is explained by the presence of residual H, C and O in the tungsten sample. A few hundred nanometer-

thick, dark-blue oxide layer appeared as a result of the oxygen contamination at high temperature. *Post-mortem* analysis with X-Ray Diffraction (XRD) and XPS revealed a predominance of orthorombic and monoclinic tungsten oxide phases, with an O:W ratio between 2 and 3. Using ellipsometry and a Cauchy model we could estimate an oxide thickness in the range 300-400 nm, in agreement with previous works [31, 39].

4. Impact of wall conditioning on the ammonia formation

The impact of wall conditioning on NH_3 formation was evaluated by first saturating the tungsten surface first to either H_2 or N_2 followed by a N_2 or H_2 plasmas, respectively. The objective of this experiment was to evaluate whether the atomic species previously present on the tungsten surface (i.e., H or N) would lead to the formation of NH_3. Next, the tungsten surface was conditioned with H_2, N_2 or O_2 plasmas and subsequently exposed to discharges of equimolar N_2-H_2 mixtures at the reference conditions of 3 Pa, 120 W and RT. The outcomes are discussed in this section and compared to the reference experiment obtained with a clean W surface (i.e., prior to any contamination with H_2, N_2 or O_2). These results are presented in sections 4.1-4.3. In section 4.4, the impact of a boron surface on the formation of NH_3 is discussed. Complementary experiments with XPS have been carried out and they are discussed along with the NH_3 formation results.

4.1. H_2 conditioning then N_2 plasma

The RGA signals obtained when exposing a hydrogen-contaminated surface to an N_2 plasma are displayed in Figure 4a). At the start of the N_2 discharge, there is a sudden increase of $m/z = 2$ and 17, suggesting both the removal of H_2 from the surface with a simultaneous formation of NH_3. The values of these species continuously decreased and stabilized after 30 minutes during the first discharge. The diminishing of NH_3 is explained by the limited amount of existing H at the reactor walls and its removal upon N bombardment. The highest value of detected NH_3 during these experiments corresponds to $\approx 0.62\%$ of all peaks, and therefore significantly smaller than the values obtained during reference N_2-H_2 discharges ($\approx 11.9\%$). Nevertheless, the formation of NH_3 indicates the existence of surface reactions initiated by the Eley-Rideal mechanism N + H(s)→NH(s), as considered in various simulation works [15, 20]. The presence of NH(s) on a previously H-saturated W surface, after exposing it to an N_2 plasma, was previously reported [28].

de Castro et al. performed similar experiments with D_2 conditioning, followed by an N_2 plasma [25]. They did not observe a measurable change in the RGA signal corresponding to the isotopologue ND_3 ($m/z = 20$). With these results, the authors concluded that the presence of N on the surface is the first step to form N-H (a detailed discussion on the role of N(s) is given next). However, it is important to note that the loading of the W wall with D was carried out in their work at 423 K and 500 eV, which

leads to enhanced implantation, diffusion and sputtering. In contrast, our experiments were done with H_2 plasmas at ≈ 300 K as starting temperature. As discussed before, while the loading below 500 K does not greatly influence the D retention in the W bulk, the amount of H on the surface at elevated temperatures is certainly lower when compared to an RT exposure. Moreover, the energy of the D^+ in de Castro et al. was significantly larger than in our experiments (≈ 20 eV). Hence, the average depth of implantation R_p is significantly higher for 500 eV D^+ (≈ 10 nm) than for 20 eV H^+ (≈ 1.8 nm), resulting in a lower concentration at the surface [40].

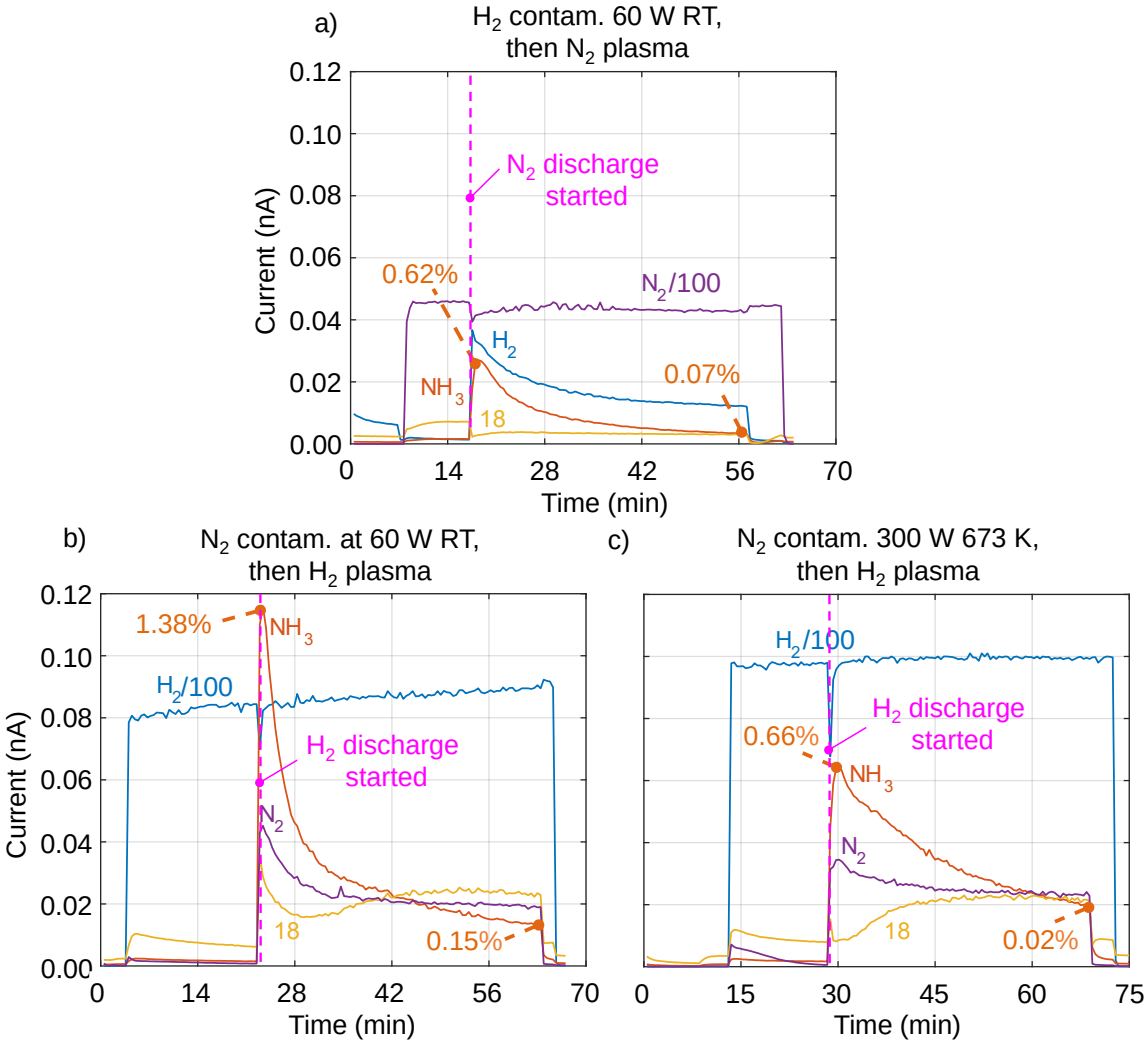

Figure 4: RGA signals obtained during single H_2 or N_2 plasmas after contamination of N_2 and H_2, respectively. In a) it is shown the run with 120 W N_2 plasma, after contamination with H_2 at 60 W and RT. In b) and c), the results obtained with H_2 plasmas of 120 W after having contaminated the foil with N_2 60 W, RT and N_2 300 W, 673 K, respectively, are shown.

4.2. N_2 conditioning then H_2 plasma

When the nitrogen-contaminated surface is exposed to an H_2 plasma alone, NH_3 is also formed as shown in Figure 4b). Similarly to the H_2 conditioning case, the NH_3 value eventually decreased down to background values after ≈ 30 min. However, the NH_3 RGA value at the beginning of the H_2 discharge was significantly higher (1.4% of all peaks) than the value obtained at the start of the N_2 discharge in the H_2 conditioning case (0.6% of all peaks). Simultaneoulsy, N_2 is observed to be removed from the surface, suggesting the replacement, up to a certain extent, of N(s) by H(s) and surface formation of NH_x either by Eley-Rideal or Langmuir-Hinshelwood. This process is consistent with the XPS data obtained after exposing a 60 W N_2-contaminated surface to 120 W plasmas of H_2 after 1, 5 and 40 min, without breaking the vacuum (section S5.2). As depicted in Figure 5, after 60 W of N_2 plasma alone a main peak at 397.1 eV appears, which is attributed to tungsten nitride. The second one above 398 eV is attributed to an N vacancy or W-N-O bonding [41, 42]. Afterwards, the increase in exposure time to 120 W H_2 plasma leads to a shift in the binding energy of N1s towards higher values, compatible with the formation of NH_x. Likewise, the N/W ratio is observed to decrease from 0.44 (after N_2 contamination) down to 0.33 (after 46 min of cumulative exposure time to H_2 plasma). At the latter conditions, the NH_x compounds amount to 80% of the N1s peak,

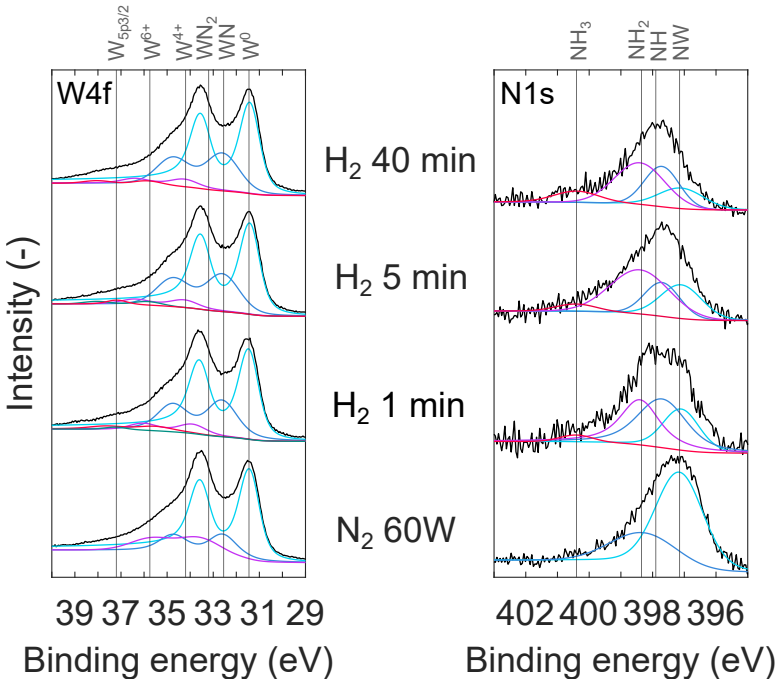

Figure 5: Core level spectra of W4f (left) and N1s (right) corresponding to the N_2-H_2 in-situ experiments with tungsten (W02-W05 in Tables S2 and S3): after 60 W N_2 at 3 Pa (W02), after 120 W, 3 Pa H_2 plasmas of 1 min in red (W03), 5 min in blue (W04) and 40 min in magenta (W05). W02 was preceded by an in-situ W coating. The binding energies of the peaks used for fitting are also shown (refer to Table S1).

	ΔE_N^{SD} (eV)	ΔE_H^{SD} (eV)
W(100)	1.168	0.671
W(110)	0.760	0.076

Table 3: Calculated activation energies for surface diffusion ΔE^{SD} of H and N on aa tungsten surface using the Density Functional Theory. Refer to SI for a more detailed description of the DFT procedure.

with a larger presence for NH_2(s) (Table S3) and the concentration of NH_3(s) is found to increase with the H_2 exposure time. These results are similar to those obtained after 20 min exposure to N_2-H_2 plasmas, with N/W $\approx$ 0.34 and around 80 % of the N1s core level due to NH_x.

While for H_2-then-N_2 the only E-R reaction leading to the formation of NH_x is H(s)+N $\rightarrow$ NH(s), for N_2-then-H_2 the following E-R reactions N(s)+H $\rightarrow$ NH(s), NH(s)+H $\rightarrow$ NH_2(s) and NH_2(s)+H $\rightarrow$ NH_3(s) are possible. Furthermore, the formation of NH_x(s) via surface processes (L-H) occur on both cases and they strongly depend on the energy barriers for surface diffusion. These quantities were determined for N and H on tungsten using the Density Functional Theory (DFT), following the procedure presented in section S6 of the SI. The results displayed in Table 3 show that the energy barriers for surface diffusion are substantially higher for surface-bound N than for surface-bound H. Consequently, while in the H-contaminated surface there is a larger probability that the more mobile H(s) will combine with each other to form H_2, in the reverse scenario the H(s) atoms will bond with the majority N(s) at a faster rate than each N(s) will recombine with another N(s). In sum, the larger number of reaction channels and the differences in surface diffusion energy barriers for H and N will contribute to a larger formation of NH_3 in the N_2-then-H_2 case.

A significantly higher presence of NH(s), NH_2(s) and NH_3(s) on a N-contaminated W surface, when compared to the reverse procedure, was reported by Ben Yaala et al. [28]. With similar experiments, de Castro et al. observed a gradual decrease of the peak $m/z = 20$ corresponding to the deuterated isotopologue [25]. These observations were attributed to an enhanced D retention in presence of tungsten nitride layers, possibly leading to a higher interaction between N and D. However, the higher D retention was reported to take place when the nitride layers are formed at 500 K, while no impact was observed at 300 K [43]. Figure 4b) displays the values obtained after subjecting the W surface to an N_2 plasma at 300 K, while the same experiment done after contaminating the walls with nitrogen at 673 K led to a NH_3 signal below 0.7% during the whole H_2 discharge (Figure 4c)). When comparing Figures 4b) and c), we also observe that a lower amount of N_2 is removed from the surface, which is explained by the formation of more stable tungsten nitrides at elevated temperatures. Thus, the lower availability of weakly adsorbed N on the W surface seems to decrease the amount of NH_3 formed. The subsequent Ar cleaning revealed a larger amount of H_2 being removed with the W surface contaminated at 673 K with N_2 than with the contamination at RT (Figure 6).

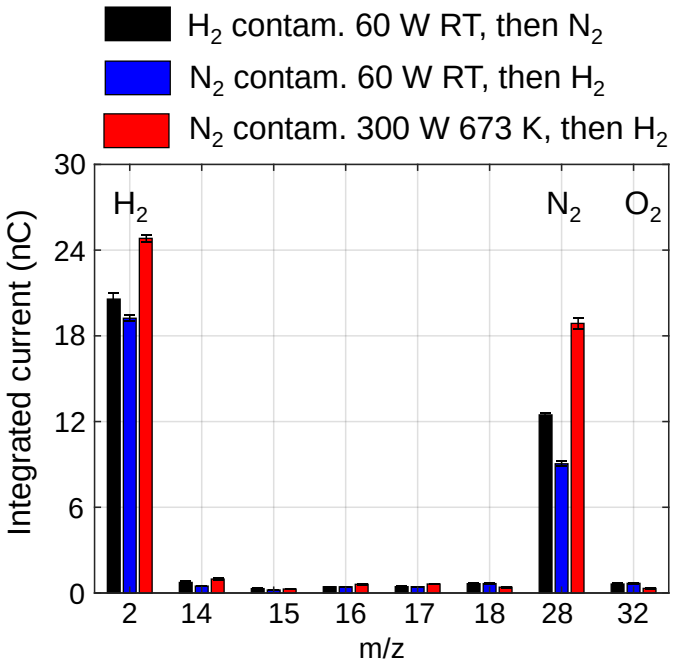

Figure 6: Integrated current obtained during Ar cleaning after the H_2-then-N_2 and N_2-then-H_2 plasma experiments. These results correspond to the data presented in Figure 4a) for H_2 then N_2 (black), 4b) for N_2 (60 W, RT) then H_2 (blue) and 4c) for N_2 (300 W, 673 K) then H_2 (red).

These observations are inline with the increased retention of H when the nitridation occurs at elevated temperatures.

4.3. H_2, N_2 and O_2 conditioning then N_2-H_2 plasma

Figure 7 displays the steady-state percentage of the signals of NH_3 and 18 in respect to all relevant signals (i.e., H_2, N_2, NH_3 and $m/z = 18$) obtained during equimolar N_2-H_2 plasmas at 3 Pa and 120 W, after having contaminated the W foil with H_2, N_2 and O_2. The values obtained before contamination are also given for reference ("Ref."). The raw data of the experimental runs for all four cases are presented in section S3 of the SI. After exposing the surface to a 2 h long H_2 plasma at RT, the steady-state percentage of NH_3 generated with an N_2-H_2 plasma was found to be somewhat lower ($\approx 10.3\,\%$) than the reference value ($\approx 11.9\,\%$). At the beginning of the discharge, most of the H atoms on the W surface are expected to be released as H_2, by direct sputtering, E-R (H + H(s)$\rightarrow H_2$) and/or L-H recombination (H(s) + H(s)$\rightarrow H_2$). A fraction of them will react with N via E-R to form NH(s). Simultaneously, the free adsorption sites are occupied by N and H atoms from the plasma volume, allowing the formation of NH(s), NH_2(s) and NH_3. The steady-state is reached within a few minutes after the discharge has started, similarly to the pristine case (Figure S6). The lower % of NH_3 at steady-state may be attributed to the role played by the atomic H present in the bulk of the W foil, which accumulated during the contamination procedure, as confirmed by TDS

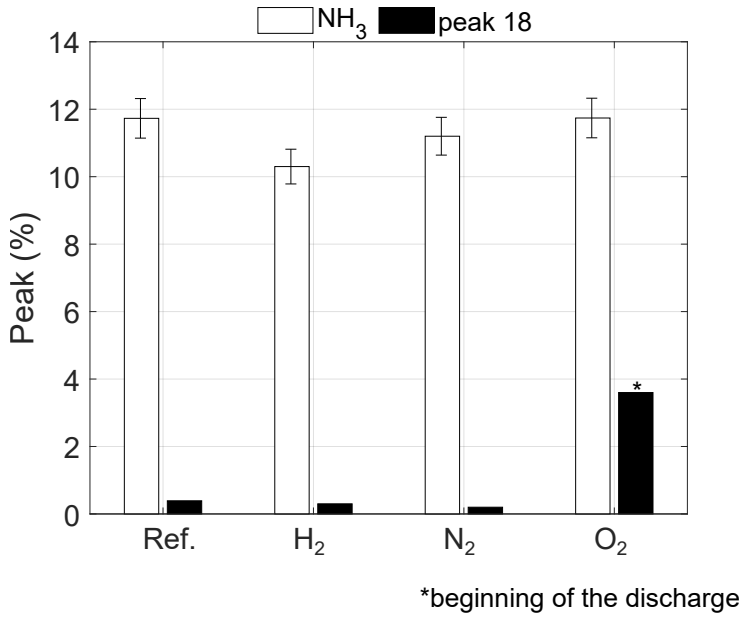

Figure 7: Percentage of NH_3 and peak $m/z = 18$ in respect to all peaks in the spectrum ($m/z = 2, 17, 18, 28$). Results obtained during an N_2-H_2 discharge at the reference conditions (50-50 mol%, 3 Pa, 120 W) after contaminating the walls with H_2, N_2 and O_2 plasmas. Contamination carried out with H_2 (RT, 60 W), N_2 (673 K, 300 W) and O_2 (673 K, 300 W) plasmas. "Ref." corresponds to the values obtained with a clean surface.

carried out after the experiment (Figure 8b)). In this scenario, H from the bulk may diffuse back to the surface and contribute to a slightly higher recombination rate at the surface (H(s) + H(s)→H_2). Indeed, Shah et al. postulated that H dissolved in the sub- and sub-sub-surface layers may play an important role in the NH_3 formation [44]. Nevertheless, with a typical experimental uncertainty of 5% relative, the effect of H_2 conditioning on NH_3 formation is considered to be small.

Figure 7 shows that the percentage of NH_3 is as well only slightly affected by the previous contamination of the reactor walls with a 2 h long, 673 K N_2 plasma. At the beginning of the discharge, an important fraction of N(s) recombines with N from the plasma volume via E-R, as a result of its high recombination rate [20], while the remaining N(s) may readily combine with H to form NH(s). After a few minutes, the production of NH_3 has reached the steady-state. The Ar cleaning that followed revealed a similar removal of H_2 and N_2 with both H- and N-contaminated surfaces (Figure 8), and in the same range of the values obtained with a clean surface (Figure 2). The major difference is the higher removal of H during TDS with H-contaminated surface, which is attributed to the higher H inventory in the bulk due to diffusion. These results hence suggest that a W surface, previously conditioned with H_2 and N_2, quickly evolves to an environment similar to that existing with a clean surface.

The presence of the tungsten oxide layer has also no impact on the formation of NH_3,

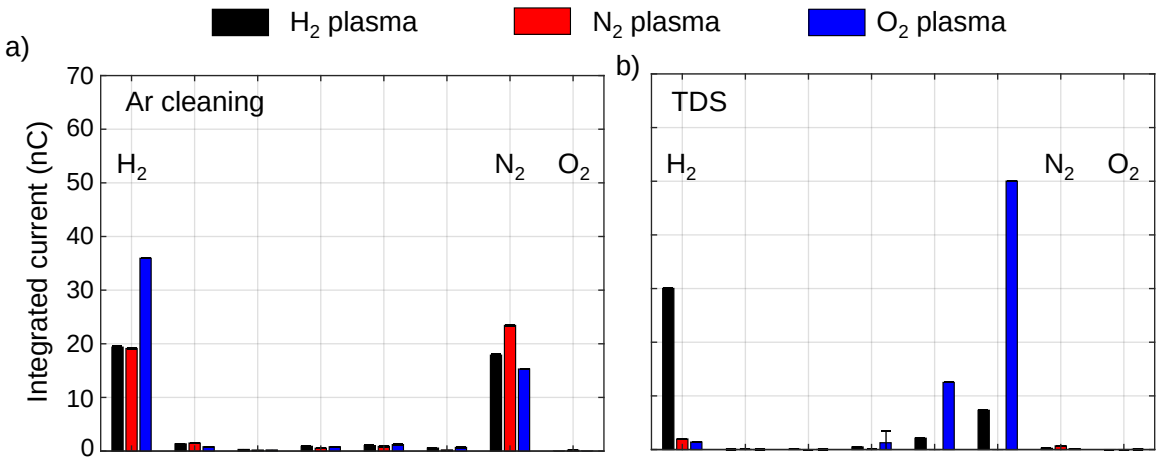

Figure 8: Integrated current obtained during Ar cleaning (left) and TDS (right) after N_2-H_2 plasmas generated at the reference conditions (50-50 mol%, 3 Pa, 120 W) with previously contaminated walls. Contamination carried out with H_2 (RT, 60 W, black), N_2 (673 K, 300 W, red) and O_2 (673 K, 300 W, blue) plasmas.

as displayed in Figure 7. The only difference in respect to the remaining experiments is the relatively high presence of peak 18 (3.6% of all peaks) at the beginning of the N_2-H_2 discharge (Figure S6). Nevertheless, after 20 min of discharge, the peak 18 reached 0.7% of all peaks, in the range of the values obtained with the other experiments. The peak 18 is therefore attributed to H_2O as a result of the interaction between O and H at the surface. Interestingly, the Ar cleaning done after the experiment showed the highest amount of H_2 to be sputtered away, while H_2O was the major species during TDS (Figure 8). These results suggest that the higher retention of H on the surface contributed to the partial reduction of the oxide layer during TDS, in very good agreement with the recent work of K. Kremer et al. [45]. These results seem to corroborate those of Matsunami et al. [46], in which they observed a larger D uptake inside 0.5 µm-thick WO_3 films (grown on a 0.2 mm-thick W sheet) when compared to a W surface. Indeed, after the experiment we observed a low amount of H_2 removed with TDS. These observations are in stark contrast with the results obtained with a clean W surface (left-hand side plots of Figure 2), suggesting that the oxide layer prevented H diffusion into the W bulk. K. Kremer et al. convincingly propose the existence of a relatively large solution barrier between the WO_3 layer and W, which prevents the diffusion of thermalized D atoms into the W bulk [45]. In this work, the authors also show that deuterium remains highly mobile inside the WO_3 layer, which is likely to be benefitial for the formation of ammonia.

The surface processes involving adsorbed H and N, via E-R and/or L-H, are considered to be pivotal to explain the NH_3 formation rates reported in the literature [15, 17–20]. To gain further insights on the processes occurring at the surface level we used Density Functional Theory (refer to section S6 for more details) to compare the

	ΔE_N^{ad} (eV)	ΔE_H^{ad} (eV)
W(100)	−8.46	−3.72
WO_3(001)	−2.09	−3.31

Table 4: Adsorption energies of N and H on W(100) and WO_3 surfaces calculated using the Density Functional Theory. Refer to SI and [29] for a more detailed description of the DFT procedure.

adsorption energies of nitrogen and hydrogen on tungsten oxide are compared to those of a pure tungsten represented by the W(100) surface in table 4. While the H adsorption energies are quite similar on both W(100) and WO_3, N is found to be significantly less adsorbed on WO_3. Since the concentration of NH_3 measured before and after the oxidation process is similar, these results are inline with previous observations that the adsorption of N on the surface is not rate-limiting at low pressures. As discussed in [21], surfaces with different N adsorption energies impact the mechanistic steps leading to NH_3 formation, albeit with limited impact on their production rates.

4.4. Boron coating then N_2-H_2 plasma

A new tungsten foil was coated with boron by means of magnetron sputtering and installed in the ammonia chamber to investigate the effect of B on the formation of ammonia. In these experiments, the discharge was generated at the reference conditions of 50-50 mol% N_2-H_2, 3 Pa and 120 W. The results before and after coating the foil with boron are shown in Figure 9. The percentage of NH_3 before B is 25% lower relative

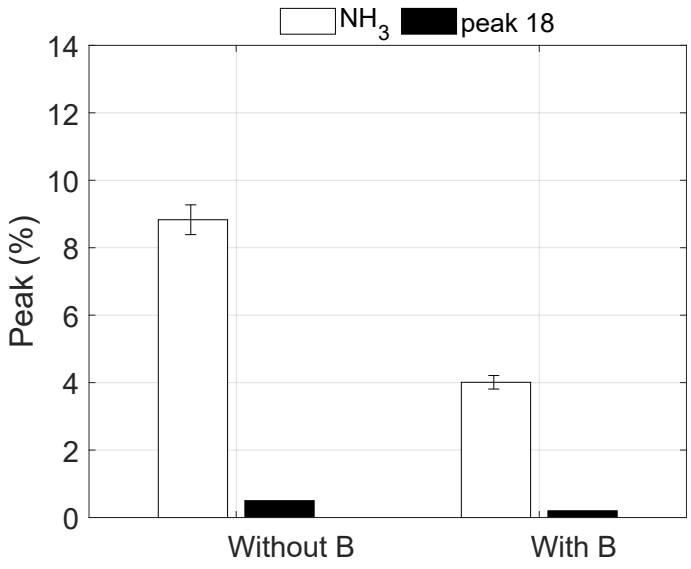

Figure 9: Percentage of NH_3 and peak $m/z = 18$ in respect to all peaks in the spectrum ($m/z = 2, 17, 18, 28$) for the tungsten foil used before and after coating it with B.

to the results obtained with the previous foil (Figure 7). This variation is within the expected fluctuations observed between different tested W samples. The boron-coated sample led to a a decrease of NH_3 by a factor of 2.

We used XPS to study in-situ the surface environment of boron after exposing it to various plasmas of N_2 alone, H_2-then-N_2, N_2-then-H_2 and N_2-H_2. The corresponding core level spectra are shown in Figure 10 and a detailed discussion on the binding energies used to fit them is given in SI, section S5.4. For all cases, we observed the formation of boron nitrides BN in both B1s and N1s peaks. Nitrogen also bonds with oxygen (N-O), which has a very similar binding energy to that of NH (around 391 eV), and therefore it is difficult to distinguish their individual contributions. The boron surface exposed to only N_2 or H_2-then-N_2 plasmas yielded similar B1s and N1s core level spectra. In these two cases, N-B and N-O are the chemical bonds responsible for the N1s peak. This behaviour is in contrast to that of tungsten, where H_2-then-N_2 leads to the formation of NH_2 on the surface [28]. On the other side, both N_2-then-H_2 and N_2-H_2 lead to a shift of the N1s peak towards higher binding energies, evidencing the presence of NH(s)

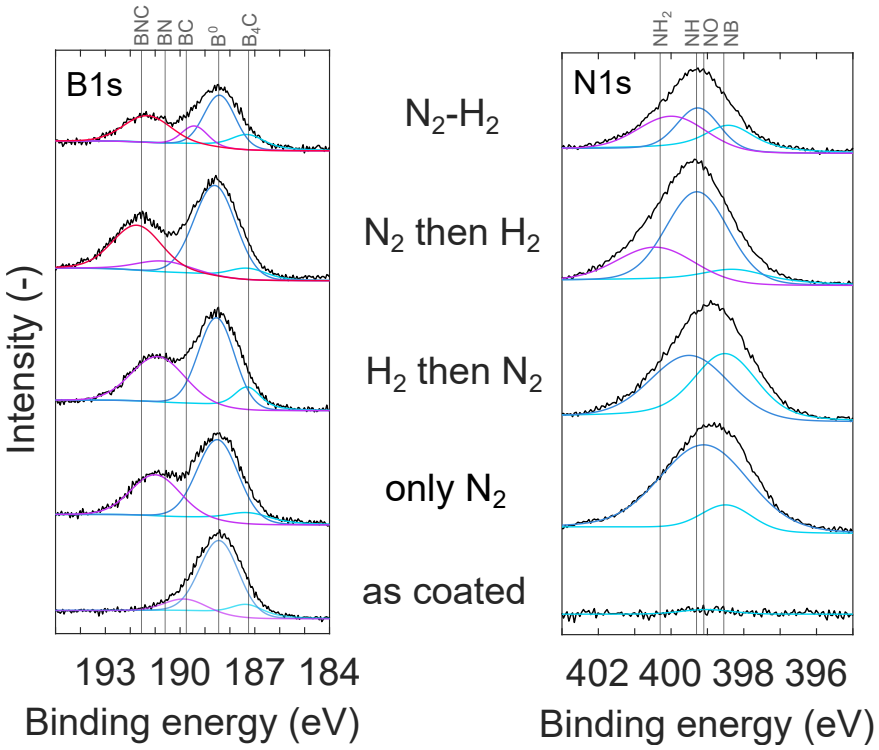

Figure 10: Core level spectra of B1s (left) and N1s (right) corresponding to the in-situ experiments with boron (B01-B05 in Tables S2 and S3): as coated (B01), after an 120 W N_2 plasma of 20 min (B02), after a sequential exposure of H_2 then N_2 at 120 W for 20 min each (B03), after a sequential exposure of N_2 then H_2 at 120 W for 20 min each (B04) and after subjecting it to a mixture of N_2-H_2 at 120 W for 20 min (B05). B01-B05 were all preceded by in-situ boron coatings. The binding energies of the peaks used for fitting are also shown (refer to Table S1).

and NH_2(s) (Table S3). Interestingly, no NH_3 (with a binding energy above 401 eV [47]) has been identified. Whereas for the tungsten case the presence of H_2 always translates into a reduction of the N/W ratio (from 0.48 with only N_2 down to 0.35 with N_2-H_2), for boron the N/B ratio remains between 0.43 and 0.46. Another important difference is that nitrogen forms bonds not only with boron (BN) but also with carbon (BNC), while on tungsten N bonds only with W (WN, W_2N or WN_2). The ex-situ experiment also showed the formation of only NH(s) and NH_2(s) when the sample was exposed to N_2-H_2 plasmas. In sum, the XPS data reveals that nitrogen bonds with boron, carbon and oxygen, although a fraction of it still reacts with H to form NH(s) and NH_2(s).

Although the XPS technique cannot resolve the bonding of hydrogen on the surface, it is known from the literature that H can form stable bonds with boron and oxygen (e.g., B-H, B-H-O). Wang et al. reported an increase in D retention and higher desorption temperatures upon formation of D-B-O bonds [48]. Moreover, Nakahata et al. showed that D bonds as B-D-B and B-D with starting decomposition temperatures around 400 K and 500 K, respectively [49]. Other studies highlight the role played by impurities (mainly O and C), and related chemical states (e.g., B-C, B-O), on the enhanced retention of hydrogen isotopes [50–52]. Indeed, carbon and oxygen are two unavoidable impurities on boron's surface: for the in-situ experiments, carbon was the major impurity with up to 15.6 at.%, while oxygen did not exceed 5.2 at.%; for the ex-situ case, the atomic concentrations of C and O were 12.3 and 24.3 at.%, respectively (Table S2). Furthermore, after the NH_3 production experiment with the boronized foil, a large amount of H_2 was removed during Ar cleaning. Figure S7 of the SI shows that the amount of H_2 removed upon Ar^+ bombardment was signifcantly larger than that with a tungsten surface, after similar N_2-H_2 plasmas. In contrast, the amount of N_2 removed from the B surface was similar to the W foil experiments. The RGA and XPS data show different aspects of what is happening on the boron surface, but both suggest a strong retention of H and N due to surface impurities. These observations thus suggest that the stable bonding of H and N inhibit the formation of important ammonia precursors either via Eley-Rideal or Langmuir-Hinshelwood mechanisms.

These results suggest that covering the tokamak walls with boron will not only reduce the amount of impurities, such as C or O, but will lead to an effective decrease, although not surpression, of ammonia upon nitrogen seeding. Ammonia has been detected in considerable amounts in the inner divertor of the AUG tokamak (up to 50 % of N_2 was converted into NH_3 [53]). Previous results demonstrated the increase of ND_3 with the increase of N_2 seeded into the plasma [54]. On the contrary, no ammonia was detected on N_2-D_2 WEST discharges [55]. Its absence was explained by the retention of N_2 inside the porous tungsten coating of the upper Cu divertor, which did not allow ND_3 formation. To the best of our knowledge, the role of boronized walls on ammonia formation was not investigated in neither of the tokamaks. The results so far available in the literature do not allow establishing a relation between the amount of NH_3 or ND_3 formed during tokamak discharges and the previous boron conditioning of the walls. Based on the results reported in this work, the role of boron-coated walls on ammonia

formation should be investigated in fully metallic tokamaks.

5. Conclusions

The role played by fusion-relevant contaminants for the formation of NH_3 in presence of a tungsten foil was studied. We first show that, upon argon sputtering, the main species desorbed from the tungsten surface, after subjecting it to various N_2-H_2 plasmas, are mainly N_2 and H_2. During this process, NH_3 is also detected by the RGA. N or N_2 are removed from the surface by Ar cleaning, whereas thermal desorption spectroscopy reveals a higher prevalence of H_2 and H_2O. Moreover, we discuss the formation of NH_3 during a discharge of N_2 or H_2, after having saturated the W surface with H_2 or N_2, respectively. A larger formation of ammonia was observed for the N_2-then-H_2 plasma experiment. This is explained both by the higher number of Eley-Rideal reaction channels to form NH_x, and the more efficient Langmuir-Hinshelwood surface processes, owing to the lower surface diffusion barrier of H to bond with the majority N adatoms. The evolution of the binding energy of N1s towards higher values is demonstrated in this work after exposing an N-contaminated surface to successive H_2 plasmas. The XPS results combined with the RGA data thus show that, up to a certain extent, the surface-bound N is replaced by H with the subsequent formation of NH_x.

Both the transient and steady-state formation of NH_3 with N_2-H_2 plasmas is observed to be rather independent of the chemical state of tungsten. For all cases, including that of a clean surface, the ammonia signal remained between 10 to 12% of all relevant signals. The exposure of the oxidized tungsten surface to the N_2-H_2 leads however to an important formation of H_2O at the beginning of the discharge. After 20 min, the water signal decreases to values close to the background. The sputtering of the reactor walls that followed the NH_3 formation experiments removed similar amounts of N_2 and H_2, albeit a larger amount of H was retained on the oxidized surface. These results evidence that, when exposed to similar N_2-H_2 plasmas, the surface of a contaminated tungsten foil quickly evolves towards an environment similar to that encountered in a clean surface, yielding similar NH_3 formation rates.

A substantial impact on the formation of NH_3 was however observed with the boron-coated tungsten foil. With this new surface, the amount of ammonia was reduced by half. On the one side, the XPS studies reveal that ratio of nitrogen-to-boron atoms is quite constant, regardless whether hydrogen is present in the plasma volume or previously adsorbed on the surface. Nitrogen not only bonds to boron (B-N) and surface impurities (B-N-C, N-O), but also to hydrogen to form NH and NH_2. No NH_3 has been however detected on the surface. On the other side, a large amount of hydrogen was removed upon Ar cleaning after the NH_3 formation experiment. This suggests an increased retention of hydrogen due to oxygen and carbon present on the surface. Therefore, the formation of stable H- and N-containing compounds on the surface are likely to reduce the number of H and N available to form ammonia precursors.

The results here discussed shall be confronted with detailed micro-kinetic models

capable of analysing the evolution of a previously conditioned metallic surface upon exposure to H_2, N_2 or N_2-H_2 plasmas. These studies are required to clarify the role played by the ion bombardment on the replacement of the previously adsorbed atoms by those present in the plasma volume and how this impacts the reaction pathways towards NH_3. The role played by boron and surface impurities on the formation of NH_3 shall be further investigated not only in fully metallic tokamaks, but also in the context of ammonia formation in low-temperature and low-pressure plasmas. The detailed understanding of the lower production of NH_3 with boron may help clarifying the rate-limiting reactions in the catalytic formation of ammonia.

References

[1] Pitts R, Bonnin X, Escourbiac F, Frerichs H, Gunn J, Hirai T, Kukushkin A, Kaveeva E, Miller M, Moulton D, Rozhansky V, Senichenkov I, Sytova E, Schmitz O, Stangeby P, Temmerman G D, Veselova I and Wiesen S 2019 *Nuclear Materials and Energy* **20** 100696

[2] Kallenbach A, Bernert M, Dux R, Casali L, Eich T, Giannone L, Herrmann A, McDermott R, Mlynek A, Müller H W, Reimold F, Schweinzer J, Sertoli M, Tardini G, Treutterer W, Viezzer E, Wenninger R and and M W 2013 *Plasma Physics and Controlled Fusion* **55** 124041

[3] Schweinzer J, Sips A, Tardini G, Schneider P, Fischer R, Fuchs J, Gruber O, Hobirk J, Kallenbach A, McDermott R, Neu R, Pütterich T, Rathgeber S, Stober J and and J V 2011 *Nuclear Fusion* **51** 113003

[4] Kreter A, Nishijima D, Doerner R, Freisinger M, Linsmeier C, Martynova Y, Möller S, Rasinski M, Reinhart M, Terra A, Torikai Y and Unterberg B 2019 *Nuclear Fusion* **59** 086029

[5] Neuwirth D, Rohde V, Schwarz-Selinger T and Team A U 2012 *Plasma Physics and Controlled Fusion* **54** 085008

[6] Drenik A, Oberkofler M, Alegre D, Kruezi U, Brezinsek S, Mozetic M, Nunes I, Wischmeier M, Giroud C, Maddison G and Reux C 2015 *Journal of Nuclear Materials* **463** 684–687

[7] Drenik A, Alegre D, Brezinsek S, de Castro A, Kruezi U, Meisl G, Mozetic M, Oberkofler M, Panjan M, Primc G, Resnik M, Rohde V, Seibt M, LTabarés F, Zaplotnik R, the ASDEX-Upgrade team, the EUROfusion MST1 team and the JET contributors 2017 *Fusion Engineering and Design* **124** 239–243

[8] Ben-Yaala M, Marot L, Steiner R, Moser L, Temmerman G D, Porosnicu C, Lungu C, Oberkofler M and Meyer E 2018 *Nuclear Fusion* **58** 106012

[9] Temmerman G D, Baldwin M, Anthoine D, Heinola K, Jan A, Jepu I, Likonen J, Lungu C, Porosnicu C and Pitts R 2017 *Nuclear Materials and Energy* **12** 267–272

[10] Wilson J, Becnel J, Demange D and Rogers B 2019 *Fusion Science and Technology* **75** 794–801

[11] Wilson J, Becnel J, Demange D and Rogers B 2019 *Fusion Science and Technology* **75** 802–809

[12] Gómez-Ramírez A, Cotrino J, Lambert R M and González-Elipe A R 2015 *Plasma Sources Science and Technology* **24** 065011

[13] Iwamoto M, Akiyama M, Aihara K and Deguchi T 2017 *ACS Catalysis* **7** 6924–6929

[14] Shah J, Wang W, Bogaerts A and Carreon M L 2018 *ACS Applied Energy Materials* **1** 4824–4839

[15] Carrasco E, Jiménez-Redondo M, Tanarro I and Herrero V J 2011 *Physical Chemistry Chemical Physics* **13** 19561

[16] Hong J, Prawer S and Murphy A B 2017 *ACS Sustainable Chemistry & Engineering* **6** 15–31

[17] Gordiets B, Pinheiro C M F M J and Ricard A 1998 *Plasma Sources Science and Technology* **7** 363–378

[18] Gordiets B, Pinheiro C M F M J and Ricard A 1998 *Plasma Sources Science and Technology* **7** 379–388

[19] Body T, Cousens S, Kirby J and Corr C 2018 *Plasma Physics and Controlled Fusion* **60** 075011

[20] Jiménez-Redondo M, Chatain A, Guaitella O, Cernogora G, Carrasco N, Alves L L and Marques L 2020 *Plasma Sources Science and Technology* **29** 08503
[21] Yamijala S S R K C, Nava G, Ali Z A, Beretta D, Wong B M and Mangolini L 2020 *Journal of Physical Chemistry Letters* **11** 10469–10475
[22] de Castro A, Alegre D and Tabarés F L 2015 *Journal of Nuclear Materials* **463** 676–679
[23] Laguardia L, Caniello R, Cremona A, Dellasega D, Dell'Era F, Ghezzi F, Gittini G, Granucci G, Mellera V, Minelli D, Pallotta F, Passoni M, Ricci D and Vassallo E 2015 *Journal of Nuclear Materials* **463** 680–683
[24] de Castro A, Alegre D and Tabarés F L 2017 *Nuclear Materials and Energy* **12** 399–404
[25] de Castro A and Tabarés F L 2018 *Vacuum* **151** 66–72
[26] Laguardia L, Caniello R, Cremona A, Gatto G, Gervasini G, Ghezzi F, Granucci G, Mellera V, Minelli D, Negrotti R, Pedroni M, Realini M, Ricci D, Rispoli N, Uccello A and Vassallo E 2017 *Nuclear Materials and Energy* **12** 261–266
[27] Ben-Yaala M, Scherrer D F, Saeedi A, Moser L, Soni K, Steiner R, Temmerman G D, Oberkofler M, Marot L and Meyer E 2019 *Nuclear Fusion* **60** 016026
[28] Ben-Yaala M, Saeedi A, Scherrer D F, Moser L, Steiner R, Zutter M, Oberkofler M, Temmerman G D, Marot L and Meyer E 2019 *Physical Chemistry Chemical Physics* **21** 16623–16633
[29] Antunes R, Steiner R, Romero-Muñiz C, Soni K, Marot L and Meyer E 2021 *ACS Applied Energy Materials* **4** 4385–4394
[30] Cifuentes S C, Monge M A and Péreza P 2012 *Corrosion Science* **57** 114–121
[31] Addab Y, Martin C, Pardanaud C, Khayadjian J, Achkasov K, Kogut D, Cartry G, Giacometti G, Cabié M and Gardarein J L 2016 *Physica Scripta* **T167** 014036
[32] Marot L, Temmerman G D, Thommen V, Mathys D and Oelhafen P 2008 *Surface and Coatings Technology* **202** 2837–2843
[33] Keinonen J, Räisänen J and Anttila A 1984 *Applied Physics A* **35** 227–232
[34] Schmid K, Manhard A, Linsmeier C, Wiltner A, Schwarz-Selinger T, Jacob W and Mändl S 2010 *Nuclear Fusion* **50** 025006
[35] Zhang X, Wu Y, Mu B, Qiao L, Li W, Li J and Wang P 2017 *Journal of Nuclear Materials* **485** 1–7
[36] Uccello A, Ghezzi F, Laguardia L, Caniello R, Dellasega D, dell'Era F, Torre D D, Donnini R, Granucci G, Mesto E, Minelli D, Passoni M, Pedroni M, Pezzoli A and Ricci D 2020 *Nuclear Materials and Energy* **25** 100808
[37] Zhang H, Zhang X, Qiao L and Wang P 2020 *Nuclear Materials and Energy* **25** 100822
[38] Alimov V K, Shu W M, Roth J, Lindig S, Balden M, Isobe K and Yamanishi T 2011 *Journal of Nuclear Materials* **417** 572–575
[39] Alimov V, Tyburska, Balden M, Lindig S, Roth J, Isobe K and Yamanishi T 2011 *Journal of Nuclear Materials* **409** 27–32
[40] Eckstein W 2002 Calculated sputtering, reflection and range values Tech. rep. IPP Max Planck Institute for Plasma Physics `http://hdl.handle.net/11858/00-001M-0000-0027-4524-1`. Accessed on January 2021.
[41] Yu H, Yang X, Xiao X, Chen M, Zhang Q, Huang L, Wu J, Li T, Chen S, Song L, Gu L, Xia B Y, Feng G, Li J and Zhou J 2018 *Advanced Materials* **30** 1805655
[42] Vemuri R, Noor-A-Alam M, Gullapalli S, Engelhard M and Ramana C 2011 *Thin Solid Films* **520** 1446–1450
[43] Gao L, Jacob W, Wang P, von Toussaint U and Manhard A 2014 *Physica Scripta* **T159** 014023
[44] Shah J, Gorky F, Psarras P, Seong B, Gómez-Gualdrón D A and Carreon M L 2019 *ChemCatChem* **12** 1200–1211
[45] Kremer K, Schwarz-Selinger T and Jacob W 2021 *Nuclear Materials and Energy* **27** 100991
[46] Matsunami N, Ohno N and Tokitani M 2009 *Journal of Nuclear Materials* **390-391** 693–695
[47] Gouin X, Grange P, Bois L, L'Haridon P and Laurent Y 1995 *Journal of Alloys and Compounds* **224** 22–28

[48] Wang W, Li Q, Kobayashi M, Oya Y, Okuno K and Luo G N 2013 *Journal of Nuclear Materials* **438** S1138–S1141
[49] Nakahata T, Yoshikawa A, Oyaidzu M, Oya Y, Ishimoto Y, Kizu K, Yagyu J, Ashikawa N, Nishimura K, Miya N and Okuno K 2007 *Journal of Nuclear Materials* **367-370** 1170–1174
[50] Suzuki S, Yang Y, Yoshikawa A, Kikuchi Y, Sagara A, Oya Y and Okuno K 2009 *Journal of Nuclear Materials* **390-391** 200–202
[51] Matsuoka K, Kobayashi M, Kurata R, Osuo J, Ashikawa N, Sagara A, Oya Y and Okuno K 2011 *Fusion Science and Technology* **60** 412–416
[52] Hamada A, Kobayashi M, Matsuoka K, Suzuki M, Osuo J, Ashikawa N, Sagara A, Hatano Y, Oya Y and Okuno K 2012 *Fusion Engineering and Design* **87** 1214–1217
[53] Reichbauer T, Drenik A, McDermott R and Rohde V 2019 *Fusion Engineering and Design* **149** 111325
[54] Drenik A, Laguardia L, McDermott R, Meisl G, Neu R, Oberkofler M, Pawelec E, Pitts R, Potzel S, Pütterich T, Reichbauer T, Rohde V, Seibt M, Temmerman G D and Zaplotnik R 2019 *Nuclear Fusion* **59** 046010
[55] Loarer T, Dittmar T, Tsitrone E, Bisson R, Bourdelle C, Brezinsek S, Bucalossi J, Corre Y, Delpech L, Desgranges C, Temmerman G D, Douai D, Ekedahl A, Fedorczak N, Gallo A, Gaspar J, Gunn J, Houry M, Maget P, Mitteau R and Moreau P 2020 *Nuclear Fusion* **60** 126046

Acknowledgments

This work has been carried out within the framework of the EUROfusion Consortium and has received funding from the Euratom research and training programme 2014-2018 and 2019-2020 under grant agreement no. 633053. The views and opinions expressed herein do not necessarily reflect those of the European Commission. The authors would like to thank the Swiss Federal Office of Energy, the Swiss Nanoscience Institute, the Swiss National Science Foundation and the Federal Office for Education and Science for their Financial support.